Available online at www.sciencedirect.com
ScienceDirect
Journal of Volcanology and Geothermal Research 160 (2007) 300–318
Journal of volcanology and geothermal research
www.elsevier.com/locate/jvolgeores

# Seismicity characteristics of a potentially active Quaternary volcano: The Tatun Volcano Group, northern Taiwan

Konstantinos I. Konstantinou [a,*], Cheng-Horng Lin [b], Wen-Tzong Liang [b]

[a] *Institute of Geodynamics, National Observatory of Athens, P.O. Box 20048, 118 10, Athens, Greece*
[b] *Institute of Earth Sciences, Academia Sinica, P.O. Box 1-55, Taipei, 115 Taiwan, ROC*

Received 18 May 2006; received in revised form 5 September 2006; accepted 14 September 2006
Available online 21 November 2006

**Abstract**

The Tatun Volcano Group (TVG) is located at the northern tip of Taiwan, near the capital Taipei and close to two nuclear power plants. Because of lack of any activity in historical times it has been classified as an extinct volcano, even though more recent studies suggest that TVG might have been active during the last 20 ka. In May 2003 a seismic monitoring project at the TVG area was initiated by deploying eight three-component seismic stations some of them equipped with both short-period and broadband sensors. During the 18 months observation period local seismicity mainly consisted of high frequency earthquakes either occurring as isolated events, or as a continuous sequence in the form of spasmodic bursts. Mixed and low frequency events were also present during the same period, even though they occurred only rarely. Arrival times from events with clear P-/S-wave phases were inverted in order to obtain a minimum 1D velocity model with station corrections. Probabilistic nonlinear earthquake locations were calculated for all these events using the newly derived velocity model. Most high frequency seismicity appeared to be concentrated near the areas of hydrothermal activity, forming tight clusters at depths shallower than 4 km. Relative locations, calculated using the double-difference method and utilising catalogue and cross-correlation differential traveltimes, showed insignificant differences when compared to the nonlinear probabilistic locations. In general, seismicity in the TVG area seems to be primarily driven by circulation of hydrothermal fluids as indicated by the occurrence of spasmodic bursts, mixed/low frequency events and a *b*-value ($1.17 \pm 0.1$) higher than in any other part of Taiwan. These observations, that are similar to those reported in other dormant Quaternary volcanoes, indicate that a magma chamber may still exist beneath TVG and that a future eruption or period of unrest should not be considered unlikely.


*Keywords:* Taiwan; Seismicity; Dormant volcano; Earthquake location; Tatun

## 1. Introduction

Volcanic activity can pose a severe threat to nearby densely populated areas and to sensitive facilities such as nuclear power plants (Tilling, 1989; McBirney and Godoy, 2003). Mitigation of volcanic hazards can usually be achieved by a coordinated volcano monitoring program that encompasses a number of multidisciplinary (geophysical, geodetic, geochemical) techniques in order to detect any early signs of unrest. Many such programs have been already implemented in developed countries like Japan or the United States but most of them are restricted to volcanoes that have erupted in historical times. However, one major problem in volcanological research is the distinction between a volcano that is capable of erupting after a long repose time and one that is not. This problem, beyond its

* Corresponding author.
*E-mail address:* kkonst@gein.noa.gr (K.I. Konstantinou).

0377-0273/$ - see front matter © 2006 Elsevier B.V. All rights reserved.
doi:10.1016/j.jvolgeores.2006.09.009

academic interest, is a highly practical one since many volcanoes belonging to this category are situated next to large cities and/or critical sites around the world.

The Tatun Volcano Group (hereafter called TVG) consists of a number of Quaternary volcanoes that are located at the northern tip of Taiwan, just 15 km north of the capital Taipei and close to two nuclear power plants. In addition to that, the unique natural beauty of the area and the fact that it has been declared a national park, attracts tens of thousands of visitors every year. Its lack of eruptions during historical times was used as the main argument to suggest that it is by now an extinct volcano. In this paper we present a detailed description of the seismicity characteristics of TVG as they stem from its monitoring by a local seismic network for a period of 18 months. These observations are then used in order to draw useful conclusions about the volcano–hydrothermal system at TVG and to perform a comparison between these characteristics and those observed in other Quaternary volcanoes. Finally, a first attempt is made to address the status of this volcano (dormant versus extinct) and to consider the resulting implications.

### 1.1. Tectonic and volcanological setting

The island of Taiwan was formed as the result of the collision between the Luzon arc carried by the Philippine Sea Plate (PSP) and the continental shelf of the Eurasian Plate (EUP) as proposed by numerous authors (see for example Wu et al., 1997 and references therein) (Fig. 1a). The oblique subduction of the PSP beneath EUP at a present rate of 8.2 cm $yr^{-1}$ (Yu et al., 1997) is responsible for the formation of the Ryukyu subduction zone extending to the east of Taiwan. To the north, the Okinawa Trough (OT), the backarc basin of the Ryukyu trench, is in the process of opening as demonstrated by both GPS measurements at the Ryukyu islands and normal faulting earthquakes occurring offshore NE Taiwan (Kao and Jian, 2001). The combination of all these processes generates a complicated geotectonic environment that has attracted the attention of many geoscientists.

Volcanism in northern Taiwan is believed to be related solely to the Ryukyu subduction zone, thus being a part of the Ryukyu volcanic arc (Teng, 1996). However, more recent studies suggest that it may actually be the result of

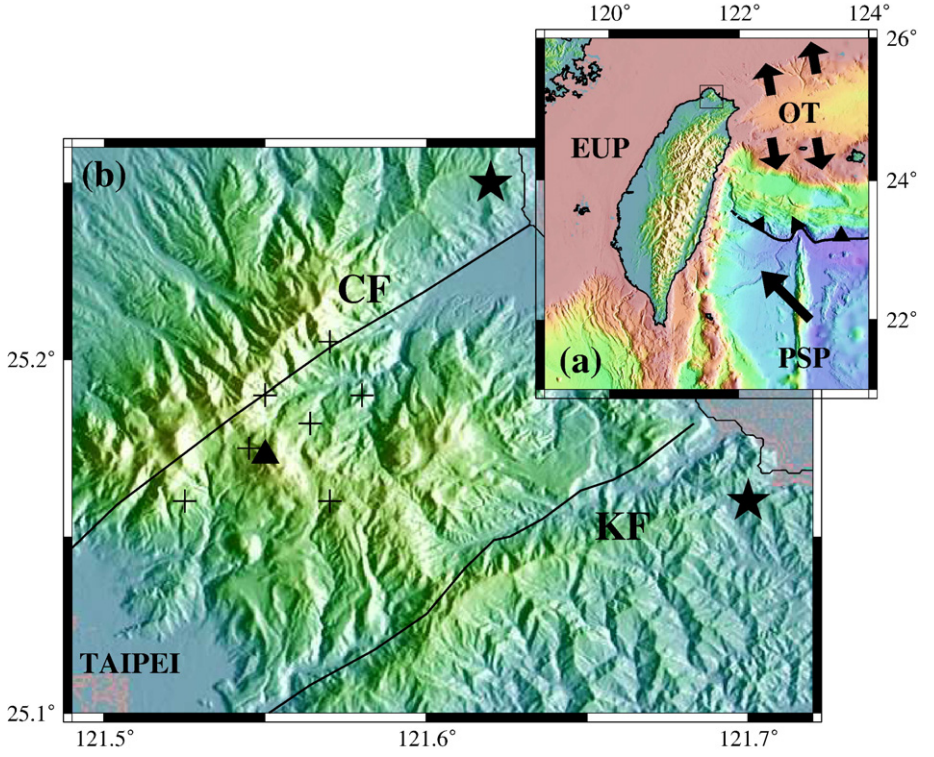


Fig. 1. (a) Map showing the regional tectonic setting and relative motion between the Philippine Sea plate (PSP) and the Eurasian plate (EUP) indicated by an arrow, as well as the opening of the Okinawa Trough (OT) backarc basin. The square in northern Taiwan shows the area of interest. (b) Map showing the area of the Tatun Volcano Group (TVG). The thick line to the south indicates the Kanchiao fault (KF), while that in the north the Chinshan fault (CF). The triangle represents the peak of the Chihsinshan volcanic cone (1120 m), the crosses indicate the place of hot spring/fumarole activity after Yang et al. (1999) and the stars show the positions of the two nuclear power plants. Part of the Taipei sedimentary basin can be seen at the lower left corner of the map.

post-collisional lithospheric extension due to the opening of the OT (Wang et al., 1999). The most prominent manifestation of this volcanism is TVG, a group of multivent Quaternary volcanoes built on a late Tertiary sedimentary basement and enclosed by two thrust fault systems, the Chinshan and Kanchiao faults (Fig. 1b). Based on fission track K–Ar/Ar–Ar radiometric dating of 80 volcanic rock samples compiled by Song et al. (2000a), the eruptive activity of TVG seems to consist of three main stages: an early eruptive stage of andesitic lava effusion between 2.8–2.5 Ma followed by a quiescent period; sparse volcanic activity that produced small amounts of lava and pyroclastic material between 1.5–0.8 Ma; and finally a major eruptive stage with the production of large amounts of andesitic lava and only few pyroclastic breccias between 0.8–0.3 Ma. Volcanic activity appears to have ceased at about 0.2 Ma ago, a date that has been used as an argument for suggesting that TVG is by now extinct.

The nearby Taipei sedimentary basin has recorded these episodes of volcanic activity through the deposition of the eruptive products, allowing us to have a more detailed picture of the eruptive behaviour of TVG. The products found in the Taipei basin strata include volcanoclastic material in fluvial deposits, lahar deposits, tuffaceous sediments and volcanic glasses stemming from ash deposits (Song and Lo, 1995; Chen et al., 1995a,b; Tsao et al., 2001). Taking into account the relative quantities of these products and of andesitic lava, it appears that the eruptive style of TVG was mainly effusive or 'silent' rather than explosive (Song et al., 2000a). However, the most important finding in the Taipei basin deposits is the presence of ash in sedimentary formations that are younger than about 20 ka along with grains of charcoals (Chen and Lin, 2000, 2002). The mineral chemistry analysis of the ash indicates that the most probable source is TVG, while the age of the charcoals derived from $^{14}C$ dating suggests that they represent *in situ* deposition materials. It is speculated that the charcoals originated from forest fires that were triggered by the volcanic eruptions. On the other hand, the measurement of the $^{3}He/^{4}He$ isotope ratio of fumarolic gas showed that more than 60% of the He composition comes from a deep magmatic source beneath TVG (Yang et al., 1999). It is therefore concluded that volcanism at TVG during the last few thousands years might have been continuous and in the form of small scale eruptions.

### 1.2. Previous geophysical studies

Tomographic imaging studies for the whole of Taiwan have shown the existence of abnormally low P-wave velocities around the area of TVG (Roecker et al., 1987; Rau and Wu, 1995; Ma et al., 1996; Kim et al., 2005a). Even though low resolution did not permit the delineation of any specific low velocity bodies in the upper crust, the authors speculated that some percentage of melt may still be present beneath TVG. In a smaller scale study over northern Taiwan, Chen et al. (2002) used data from the national seismographic network maintained by Taiwan's Central Weather Bureau (hereafter called CWB), in order to obtain three-dimensional images of body wave attenuation. The results showed high P- and S-wave attenuation at the first 15 km beneath TVG ($Q \sim 90–200$) that the authors tentatively interpreted as resulting from a partially molten body. Two seismic experiments covering the broader area of TVG and northern Taiwan were performed in 1989–1990 (Chen and Yeh, 1991; Chen et al., 1995a,b) and in 1996–2000 (Yeh et al., 1998) by deploying three-component short period seismometers. Unfortunately, the data analysis in both studies was limited in identifying only tectonic events and not volcanoseismic signals. Also, the resulting earthquake locations appeared quite diffuse, not allowing any interpretation of the hypocentral distribution.

More recently Kim et al. (2005b) studied the seismicity around TVG using seismic data recorded by various regional networks (the Taiwan Telemetered Seismic Network operating from 1973 until 1991, the Taiwan Seismic Network operating from 1991 until now and the Broadband Array in Taiwan for Seismology operating from 1996 until now). The authors observed the repeating occurrence of several swarms that consisted of numerous small earthquakes not reported in the CWB catalogue. Even though the exact location of these events was not possible due to the small number of available arrival times, it was suggested that this activity is related to subsurface volcano–hydrothermal processes. In support of this conclusion, Kim et al. (2005b) also report a *b*-value for the TVG area equal to 1.22 that is in accordance with *b*-values observed in other volcanic areas around the world.

Gravity and magnetic surveys over the broader area of TVG were carried out simultaneously and their results were reported by Yang et al. (1994). The gravity survey showed that for the upper 4 km, predominantly high, positive anomalies were present and were interpreted as being caused by the density contrast between the volcanic and surrounding sedimentary rocks. The magnetic survey results also showed mostly magnetic highs except from certain areas where fumarolic activity is quite strong. This correlation was believed to be the result of the extensive hydrothermal alteration of rocks so that

ferromagnesian minerals may have been partially or completely weathered out.

## 2. Data collection and analysis

In May 2003 the Institute of Earth sciences, Academia Sinica, initiated a project for seismic monitoring of TVG funded by the National Research Council of Taiwan and the Yangminshan National Park. During the first stage of the project five seismic stations were installed, four of them equipped with both a short period three-component sensor (Lennartz LE3D) and a broadband one (Guralp CMG-3T). The instruments were recording data continuously at a sampling interval of 100 samples $s^{-1}$ while absolute timing was provided by GPS receivers. The seismic stations of this small aperture array were distributed around the Chihsinshan volcanic cone which appeared to exhibit the highest seismicity in the TVG area during the last seismic experiment (Yeh et al., 1998). In early September 2003 the second stage of the project commenced and three additional short period three-component seismometers were installed in the nearby area of Tayiokeng where most of the present day hydrothermal activity is observed. Fig. 2 shows the position of the eight seismic stations in the Chihsinshan–Tayiokeng area and Table 1 gives some details for each station separately. A preliminary analysis of the data recorded during the first stage of the project has been published by Lin et al. (2005a,b). This work will be focused on the period between October 2003 and February 2005, when all 8 stations were operational.

Table 1
List of seismic stations deployed at the TVG area for the period between September 2003 until February 2005

| Station | Lat (°N) | Lon (°E) | Elev (km) | Sensor type |
|---|---|---|---|---|
| YM01 | 25.1481 | 121.5620 | 0.488 | Le3D/CMG-3T |
| YM02 | 25.1863 | 121.5621 | 0.521 | Le3D/CMG-3T |
| YM03 | 25.1809 | 121.5314 | 0.702 | Le3D/CMG-3T |
| YM04 | 25.1552 | 121.5278 | 0.401 | Le3D/CMG-3T |
| YM05 | 25.1665 | 121.5564 | 0.740 | Le3D |
| YM06 | 25.1538 | 121.5943 | 0.445 | Le3D |
| YM07 | 25.1771 | 121.6123 | 0.456 | Le3D |
| YM08 | 25.1890 | 121.5808 | 0.342 | Le3D |

Seismic data were usually retrieved once per month during regular network maintenance and our analysis started each time by creating a daily drumplot of the vertical components for each station. Using this plot the recorded signals were first grouped in three main categories: namely teleseismic, regional and local events. Teleseismic events were identified after consulting the NEIC (National Earthquake Information Centre) database, while the same procedure was followed for the regional events using the seismicity catalogue provided by CWB. In this way, local earthquakes and other

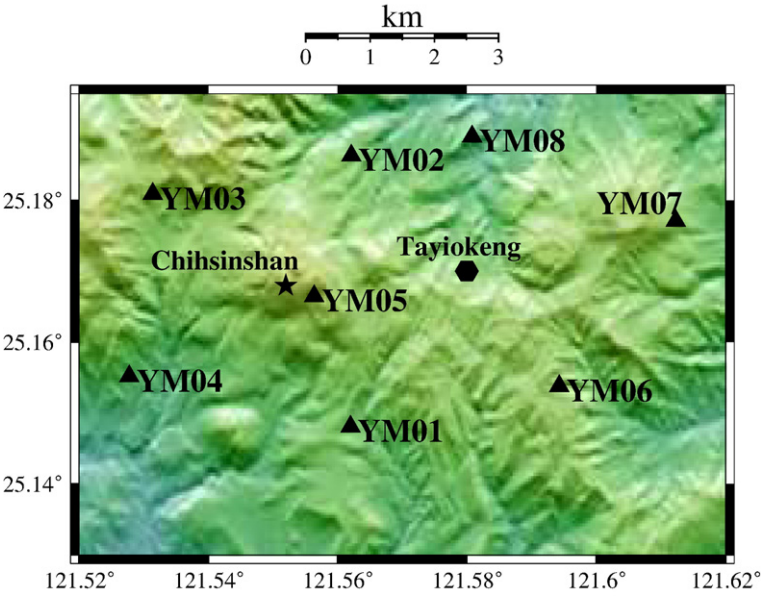


Fig. 2. Map showing the station distribution during the seismic monitoring experiment (see also Table 1). The star indicates the peak of the Chihsinshan volcanic cone and the polygon the centre of the Tayiokeng area.

volcanoseismic signals were isolated and stored every month for further analysis. These signals were classified into different groups by using a simple scheme based on the observed frequency content and waveform appearance (McNutt, 1996). Propagation effects are usually quite severe around volcanic areas and may lead to biased classification of signals, if the source–receiver distance is large and/or the signal is recorded at only a few stations. In order to avoid these complicating factors, we classified signals that were recorded clearly by at least five stations, looking carefully for time or frequency domain characteristics present at all available stations.

A description of each group resulting from this classification scheme is given below:

(1) *High frequency earthquakes*. They are characterised in the time domain by impulsive P-wave onsets and clear S-wave phases, while in the frequency domain most of the energy is concentrated in the band 1–20 Hz (Fig. 3). Of course they are similar to tectonic earthquakes observed in non-volcanic areas worldwide. Most of the seismicity observed during the 18 months of monitoring described in this study is in this category.

(2) *Spasmodic bursts*. These are continuous seismic signals of varying duration (20 s to 15 min) that consist of numerous high frequency earthquakes occurring very closely in time (Fig. 4). This kind of seismicity was quite common in the TVG area and two of the longest duration spasmodic bursts occurred between October 28–30, 2003.

(3) *Mixed frequency earthquakes*. These events have a sharp P-wave onset, no clear S-wave phase and they consist of a high frequency (up to 40 Hz) initial part, followed by a later low frequency (~5 Hz) harmonic coda (Fig. 5). Eight mixed frequency events were observed in the period between February and June 2004.

(4) *Low frequency earthquakes*. Two kinds of these events were observed in the TVG area: tornillo events have a characteristic decaying waveform that looks like a screw in a cross-section ('tornillo' is the Spanish word for screw). Their duration extends up to 40 s and consist of discrete frequencies at 2.2, 4.2, 6.2, 8.2 and 9.6 Hz (Fig. 6a). Monochromatic events have smaller durations (15–20 s) and most energy is concentrated around 3.4 Hz (Fig. 6b). Low frequency signals were

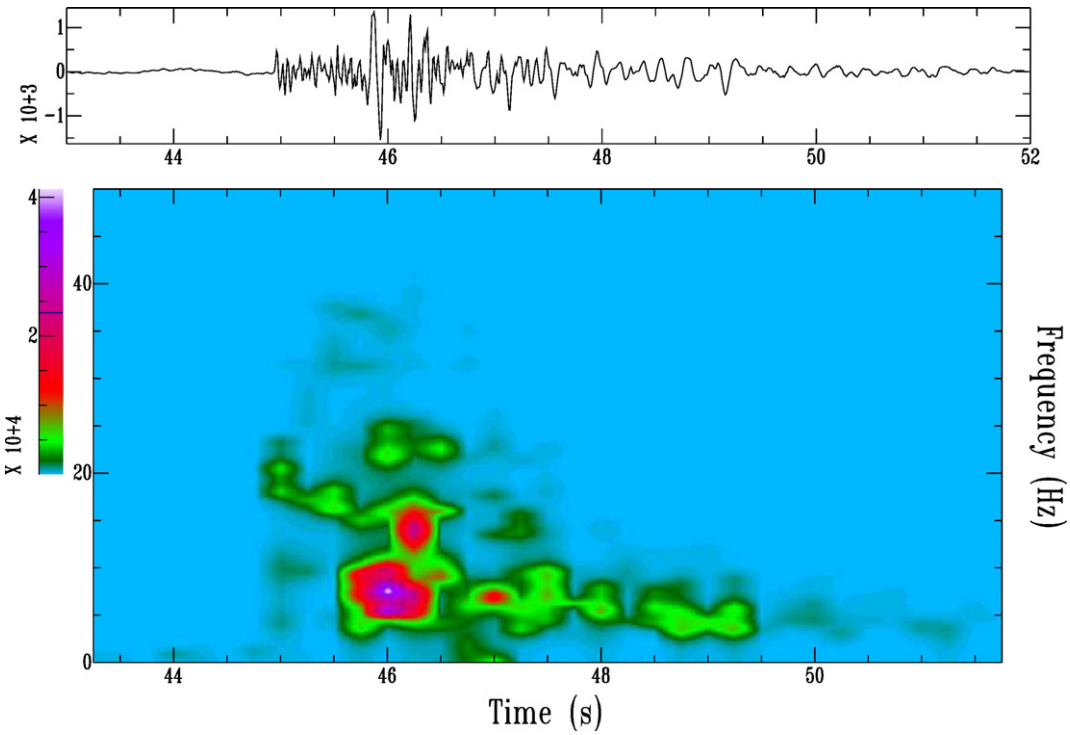


Fig. 3. Vertical velocity waveform and corresponding spectrogram for a high frequency event that occurred at September 9, 2003 11:07:43.8 (GMT) ($M_L$ 1.0). The signal was recorded at station YM05 by a short-period sensor. The spectrogram was calculated for a 0.5 s window and 50% overlap using the technique of Goldstein and Minner (1996).

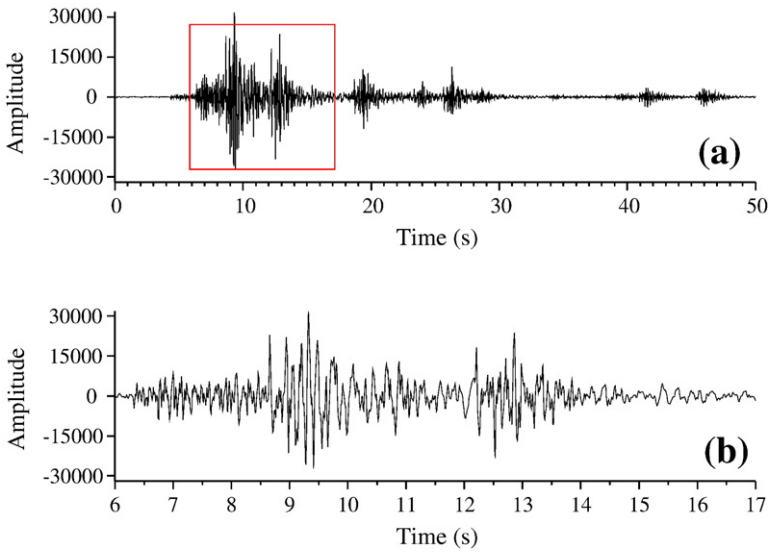


Fig. 4. (a) Vertical velocity waveform of a spasmodic burst that occurred in October 28, 2003 recorded by the short-period sensor of station YM05, (b) enhanced section of the highlighted part of the waveform shown in (a), where it can be seen that spasmodic bursts consist of ordinary high frequency events.

observed in the TVG area only in early September 2003 and consisted of 3 tornillo and 2 monochromatic events. After that period no other low frequency signal was detected, while occasionally some monochromatic signals could be seen just above noise level at the stations around Tayiokeng.

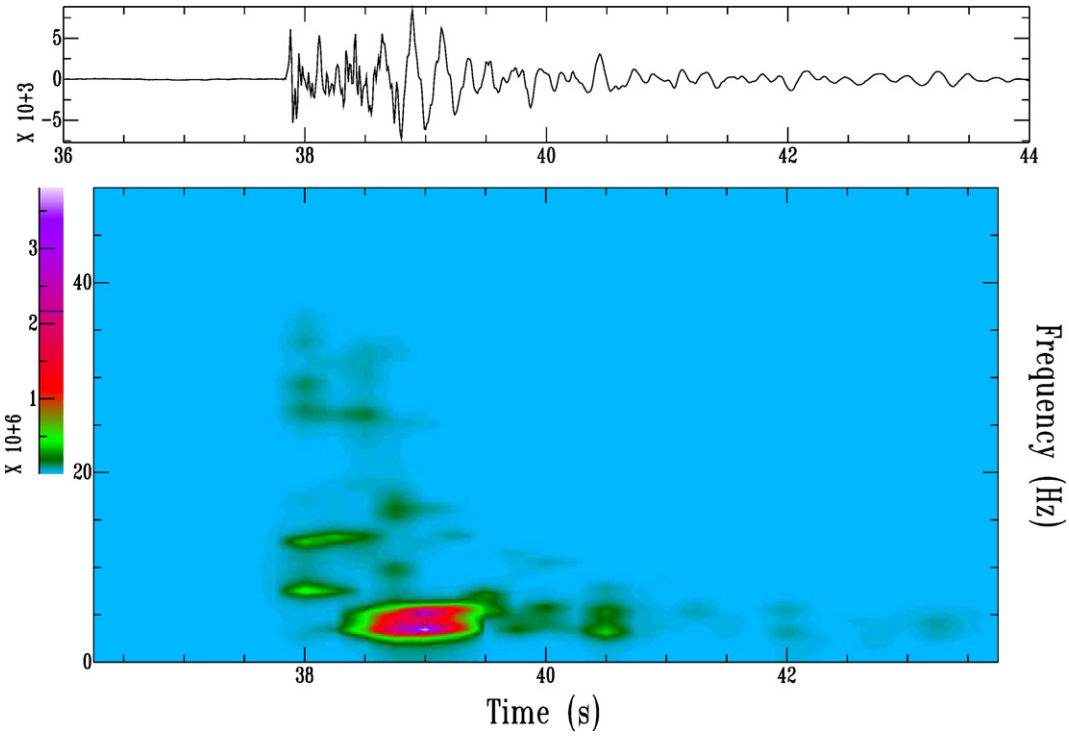


Fig. 5. Vertical velocity waveform and corresponding spectrogram for a mixed frequency event that occurred at April 2, 2004 17:50:37.17 (GMT) ($M_L$ 1.0). The signal was recorded at station YM03 by a short-period sensor. The spectrogram was calculated the same way as in Fig. 3.

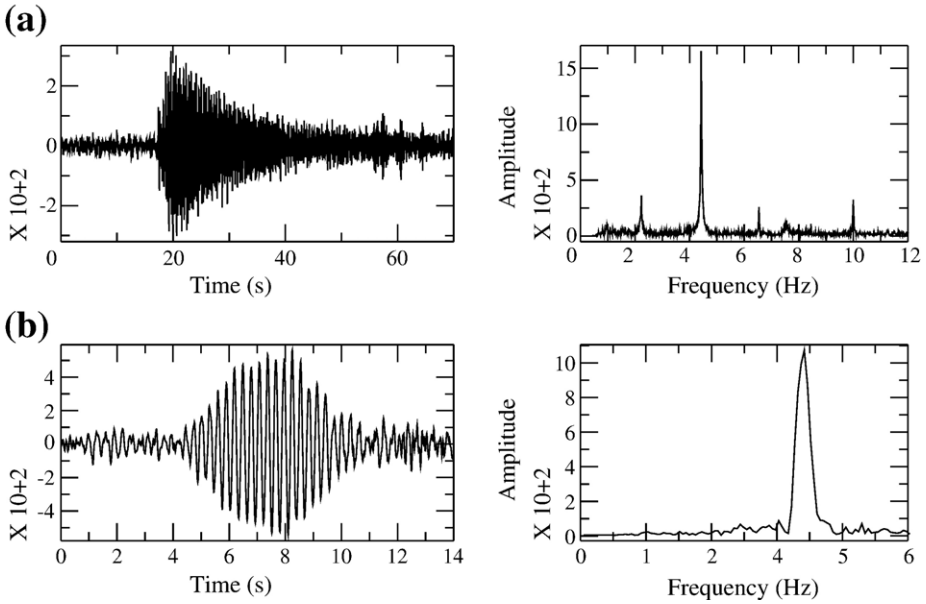


Fig. 6. Vertical velocity waveforms and corresponding amplitude spectra for (a) a tornillo event and (b) a monochromatic event recorded by short-period sensors at stations YM05 and YM02 respectively (see text for more details).

Lin et al. (2005a) analysed these signals using the Sompi method (Kumagai and Chouet, 2000 and references therein) in order to determine the frequency and quality factor of the underlying oscillations. Their results showed that a crack filled with an ash–gas or water droplet–gas mixture are the most likely candidates for explaining the large quality factors (250–1000) of these signals. These two mixtures are stable under different physical conditions (pressure and temperature) and therefore at different depths (Molina et al., 2004). Unfortunately, the authors had no constrained hypocentral locations for these low frequency events that would allow them to decipher which one is the most likely mixture.

Subsequently and for the purpose of source location, we use the short-period wave-forms to manually pick a total of 211 events (144 high frequency events, 59 events belonging to spasmodic bursts and 8 mixed frequency events). For high frequency or spasmodic burst events at least five P- and one S-phase pick was required for selection, while at least five P-phases was the requirement for the mixed frequency events. Fig. 7 shows the temporal distribution of all events that were included in the final dataset.

We also estimated the local magnitude ($M_L$) of these events by measuring on a standard Wood–Anderson simulated trace their maximum peak-to-peak amplitude on the horizontal components at each station. An attenuation function derived for the Taiwan area and for epicentral distances smaller than 80 km was used in these calculations (see Shin, 1993). This procedure resembles the one used by CWB for local magnitude estimation, therefore our $M_L$ estimates are directly comparable to those found in the CWB catalogue. In fact, for 10 events that were common in both seismicity catalogues we found that our magnitude values are in

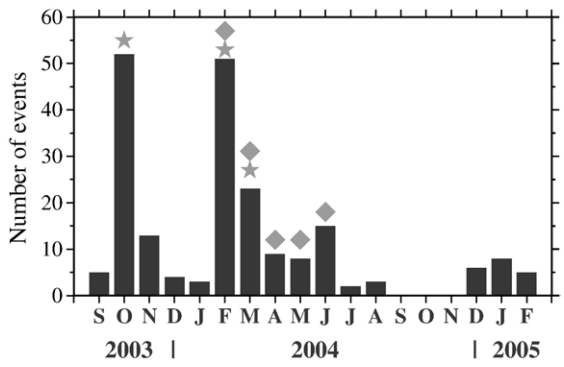


Fig. 7. Histogram showing the temporal variation of the number of picked events per month for the whole of the observation period. The stars on top of some bars indicate the occurrence during that month of a series of spasmodic bursts. The diamonds represent the occurrence of mixed frequency events. The almost zero number of events from July to December 2004 is due to network problems that did not allow a continuous recording of data at all stations.

Table 2
Velocity model used for initial earthquake locations

| Depth (km) | $V_P$ (km s$^{-1}$) |
|---|---|
| 1.0 | 4.07 |
| 2.0 | 4.55 |
| 3.0 | 5.12 |
| 5.0 | 5.39 |
| 7.0 | 5.98 |
| 9.0 | 6.10 |
| 17.0 | 6.70 |

good agreement with those published by CWB (differences smaller than 0.1 units). The largest magnitude observed in the TVG dataset is 2.78 for an event that occurred in February 24 2004, while five more events in our dataset had a magnitude of 2 or greater. The estimation of the *b*-value for the high frequency earthquakes (either isolated or occurring as spasmodic bursts), yields a value of 1.17 (±0.1) for a completeness magnitude threshold of 1. This value is similar to those estimated previously for the TVG area by Wang (1988) (~1.33) and by Kim et al. (2005b) (~1.22).

## 3. Absolute earthquake locations

### 3.1. Method outline

We chose to apply a probabilistic nonlinear method for earthquake locations, by using the freely available software package NONLINLOC (Lomax et al., 2000). The algorithm implemented in this package follows the probabilistic formulation of inversion suggested by Tarantola and Valette (1982). A probabilistic solution can be expressed as *a posteriori* Probability Density Function (PDF) provided that the errors in the observations (phase picks) and in the forward problem (traveltime calculation) are Gaussian. There are several ways that such *a posteriori* PDF can be computed and for the purpose of our study we selected the Oct-Tree sampling algorithm (Lomax and Curtis, 2001) that uses recursive subdivision and sampling of cells in 3D to generate a cascade of sampled cells. A comparison between probabilistic earthquake locations obtained by NONLINLOC and those obtained by traditional linear algorithms exhibits three major differences. First, the nonlinear location algorithm is less sensitive to the problem of local minima in the solution space. Second, for events occurring outside the seismic network NONLINLOC can provide a much better constraint on the hypocentral depth and its corresponding vertical error estimate (Lomax et al., 2000). Third, the horizontal/vertical error estimates derived by linear algorithms have been found unrealistically small when compared to those obtained by NONLINLOC (Lippitsch et al., 2005).

The NONLINLOC package can utilise either a 1D or 3D velocity model but no detailed velocity information from a tomographic or a refraction seismic experiment exists for the TVG area. In order to obtain initial locations for the events in our dataset we used the 1D velocity model listed in Table 2 assuming a $V_P/V_S$ ratio of 1.723 suggested for the Taiwan region by Kim et al. (2005a). This model has been empirically compiled previously by one of the authors of this paper in an effort to accurately locate events recorded by local seismic networks in northern Taiwan (C. H. Lin unpublished work). Nevertheless, it is necessary to assess the applicability and accuracy of the velocity model used before we embark on further analysis and refinement of earthquake locations.

### 3.2. Estimation of the minimum 1D velocity model

The concept of the minimum 1D velocity model has been introduced by Kissling et al. (1994) and refers to a 1D model that yields the smallest possible uniform error for a set of well-locatable events. Furthermore, the authors developed a methodology of how to obtain such a velocity model from the P- and S-wave traveltimes of local earthquake data by simultaneously inverting for 1D velocities, hypocentre locations and station delays. The forward problem is solved by ray-tracing from source to receiver and computing direct, refracted and reflected rays passing through the 1D model while the inverse problem is solved by using a standard damped least-squares method. The freely available code VELEST (Kissling, 1995) calculates a minimum 1D model by implementing the computational scheme described above.

Prior to inverting for the minimum 1D model we screened our dataset in order to filter out any outliers and to select only well-constrained events as input to VELEST. This selection process was based on two criteria: (a) an azimuthal gap less than 180°, and (b) a root-mean-squared (rms) residual value smaller than 0.1 s. The final dataset used for the calculation of the minimum 1D model consisted of 135 events with 900 P-phase and 657 S-phase observations. Following the procedure described by Kissling et al. (1995), we used several initial models with different layers of thicknesses and velocities in order to avoid being trapped in a local minimum of the solution space. We initially chose to invert only the P-phase observations since they provide better spatial sampling and have smaller picking errors than the corresponding S-phases. After obtaining a stable solution for the P-wave velocities, we included the S-

phase observations in the inversion in order to obtain also the minimum 1D S-wave velocity structure.

Fig. 8 shows the final minimum 1D model for P- and S-waves along with the variation of $V_P/V_S$ ratio with depth. Because the hypocentral depth for the majority of selected events is shallower than 5 km, the number of rays sampling deeper crustal horizons is limited and therefore the velocity value below that depth is almost arbitrary. A comparison between this model and averaged 1D models resulting from seismic tomography studies shows greater similarity with the results published by Rau and Wu (1995) for northern Taiwan rather than the model suggested by Chen (1995) for the whole of the island (used by CWB for routine earthquake locations). It is also interesting to note the similarity between the resulting minimum 1D model and the model used for obtaining the initial event locations.

We tested the quality and stability of the minimum 1D model by randomly shifting the initial hypocentral coordinate values by 3 to 4 km before introducing them to VELEST. It is expected that if the proposed minimum 1D model represents a robust minimum in the solution space, no significant changes in velocity and event locations should occur. The average difference in latitude and longitude between the original locations and the recalculated ones are 80 and 122 m respectively, while in focal depth it is 230 m. Another way to test the quality of the velocity model is to check whether the values of the resulting station delays (relative to a reference station in the central part of the area) reflect the near-surface geology. The delays observed across our network, using station YM05 as the reference station, are listed in Table 3 for both P- and S-waves. Stations that exhibit either small positive or zero values (indicating true velocities lower than those of the 1D model), are located on volcanoclastic material and sediments. On the other hand, only two stations (YM04 and YM08) located on andesitic lavas exhibit negative values.

### 3.3. Error analysis and location results

We calculated probabilistic earthquake locations for our dataset using NONLINLOC and the minimum 1D model with its corresponding station corrections derived earlier. By default, NONLINLOC provides two kinds of hypocentre coordinates for each event: (a) one corresponding to the maximum likelihood (or minimum misfit) point of the complete nonlinear location PDF, and (b) one corresponding to a Gaussian estimate based on the covariance matrix that is obtained from samples drawn from the PDF. The Gaussian location estimate as well as the resulting confidence ellipsoid will be good indicators of the location uncertainty only if the complete, nonlinear PDF has a single maximum and an ellipsoidal form (Lomax et al., 2000).

In order to make an accurate assessment of the errors involved in our location results, we first examined the difference between the resulting maximum likelihood and Gaussian hypocentres for each event. In this way we aim at identifying events that have a distorted PDF and therefore their confidence ellipsoid estimates are biased. We found that the majority of our events exhibit

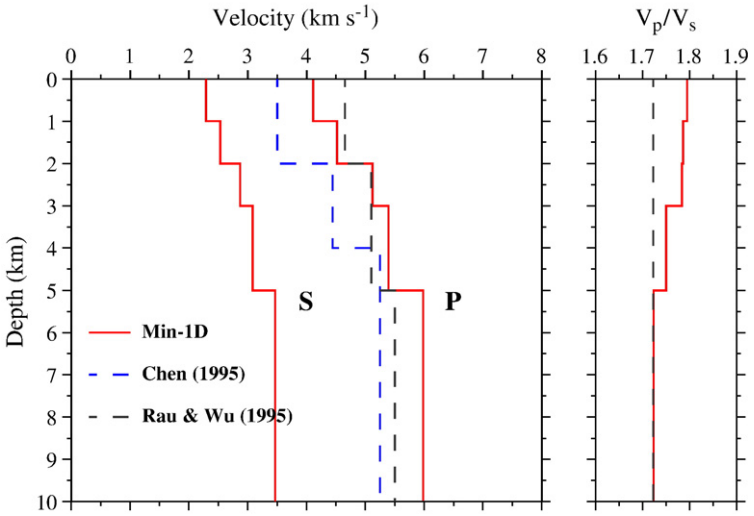


Fig. 8. Left panel: diagram showing the minimum 1D P- and S-wave velocity model for the TVG area compared with other regional velocity models. The model is well-constrained only for the upper 5 km. Right panel: the variation of the $V_P/V_S$ ratio with depth stemming from the minimum 1D model.

Table 3
P- and S-wave station corrections for the minimum 1D model relative to the reference station YM05

| Station | P-delay (s) | S-delay (s) |
|---|---|---|
| YM01 | 0.02 | 0.05 |
| YM02 | 0.02 | 0.09 |
| YM03 | 0.00 | 0.00 |
| YM04 | −0.03 | −0.15 |
| YM05 | 0.00 | 0.00 |
| YM06 | 0.01 | −0.04 |
| YM07 | 0.01 | 0.00 |
| YM08 | −0.02 | −0.11 |

horizontal differences in the range 0–200 m, vertical differences smaller than 0.5 km and quasi-ellipsoidal PDFs (Fig. 9). Larger differences coincide with events that originate at depths shallower than 1 km (mostly spasmodic burst events) where the closest station used for the location is at a distance larger than 1.5 times the focal depth (Fig. 10). This is consistent with the results of Gomberg et al. (1990) that suggest that at least one P- and one S-wave arrival time at a station within a distance of 1.5 focal depths from the source is needed for a constrained location. Based on the confidence ellipsoid dimensions of the well-constrained events, we estimate the mean absolute error in the epicentre location as 700 m and in focal depth as 1.5 km.

Fig. 11 shows a map of the distribution of probabilistic locations including two depth cross-sections. Isolated high frequency events form tight clusters at the places where most of the hydrothermal activity is observed (western part of the Chihsinshan edifice and Tayiokeng). Their hypocentres seem to form two layers beneath Chihsinshan at depths 0–2 km and 2.5–4 km, while the foci become progressively deeper in the NE direction down to a depth of approximately 6 km. On the other hand, spasmodic bursts events form one small cluster beneath Chihsinshan at depths ranging from 0 to 2 km and a second larger cluster near Tayiokeng at depths shallower than 2 km. Mixed frequency events occur very close to high frequency events and at similar depths (~2 km) with only one exception. It is also interesting to note that all seismogenesis ceases at a

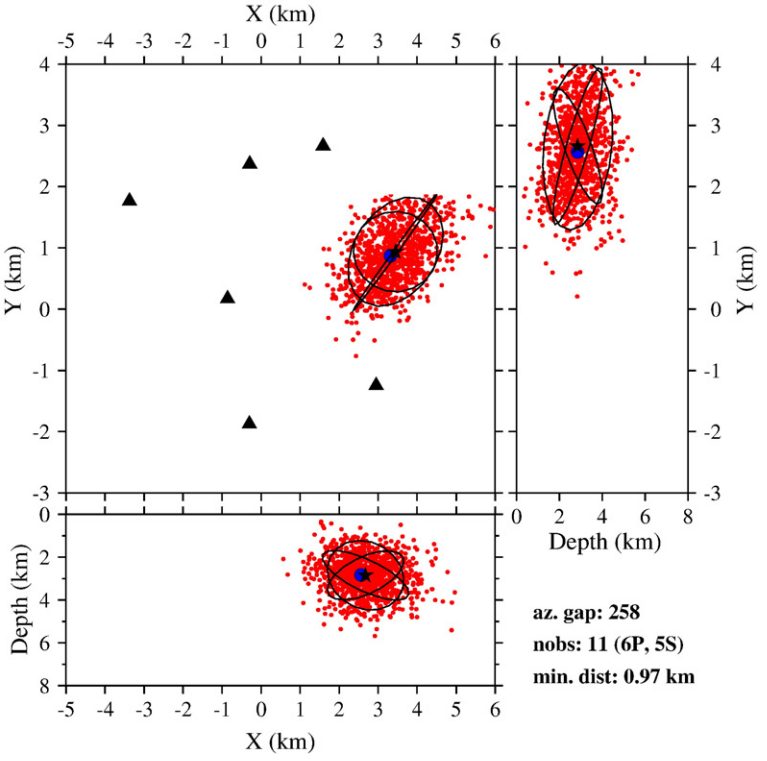


Fig. 9. Density scatter plot for a high frequency event ($M_L$ 1.5) that occurred at (GMT) 10:29:23 February 19, 2005. Black triangles represent the stations that were used for the location. The blue circle indicates the maximum likelihood location estimate, while the black star the Gaussian one. Solid black curves indicate the projection of the 68% of the confidence ellipsoid. Additional information like azimuthal gap (az. gap), number of observations used for the location (nobs) and distance to the closest station (min. dist) can be seen at the lower right corner of the plot. The closest station here lies at a distance (0.97 km) smaller than 1.5 times the focal depth of the event (2.85 × 1.5 = 4.27 km).

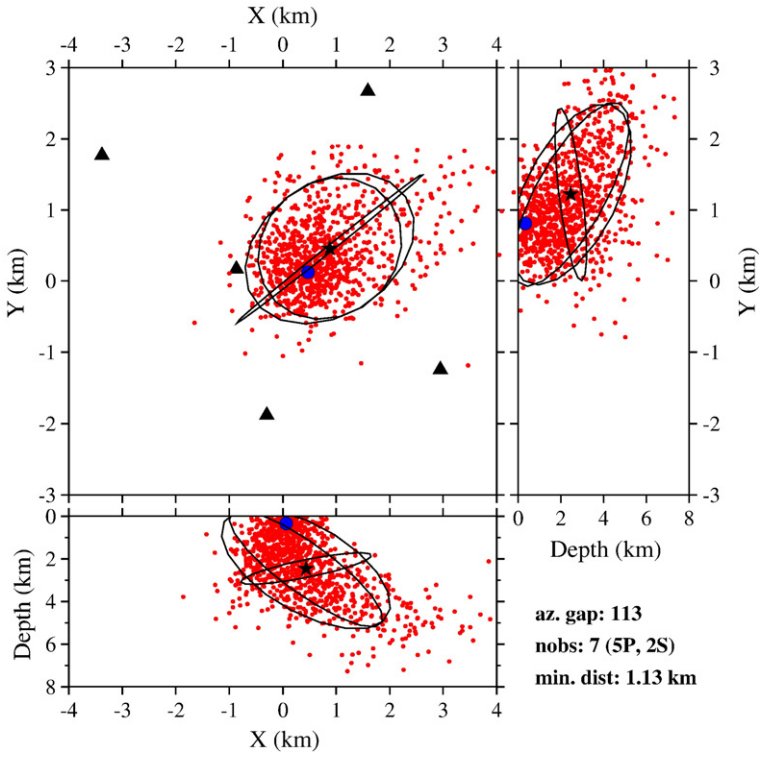


Fig. 10. Same as in Fig. 10 for a high frequency event ($M_L$ 1.0) that occurred at (GMT) 09:24:03 October 29, 2003. The closest station lies at a distance (1.13 km) larger than 1.5 times the focal depth of the event (0.33 × 1.5 = 0.49 km). This results in a non-ellipsoidal form of the sampled PDF as compared to the one in the previous figure.

depth near 4 km, with the exception of four events that occur between 5.5–7 km.

## 4. Relative earthquake locations

We further applied the double-difference method developed by Waldhauser and Ellsworth (2000) in order to obtain precise relative locations for the events of our dataset. The method tries to minimise the residuals between observed and calculated traveltime differences for pairs of events at common stations by iteratively adjusting the vector difference between the hypocentres. The algorithm makes use of any combination of ordinary picks from earthquake catalogues and/or differential traveltimes from cross-correlation of P- and/or S-phases. We calculate catalogue traveltime differences for P- and S-wave arrivals from pairs of earthquakes that are separated by less than 1 km distance. Except from the catalogue traveltime differences, we obtain differential traveltimes from correlated P-phase waveforms using the technique of VanDecar and Crosson (1990). Two waveforms were considered similar within a tapered 1 s window (100 samples) if they had a cross-correlation coefficient above 70%. Differential traveltimes were calculated when the criteria described above were satisfied at three or more stations per event pair. The distribution of cross-correlation values shows a small variation and a peak around 0.85–0.90 coherency (Fig. 12). Following Waldhauser (2001), we applied a two-stage weighting scheme: during the first stage the catalogue data are given a higher weight in order to constrain the relative position of events, while in the second stage they are down-weighted in favour of the highly accurate cross-correlation data that constrain the locations of close-by events.

From our initial dataset, 151 events were finally relocated using the double difference-method (Fig. 13). This reduction in the number of events after the relocation process is probably due to the loss of linkage for some spasmodic bursts events with quite shallow focal depths. As mentioned earlier, these events lack phases from stations close to the source and are located by the algorithm above ground ('airquakes') causing the vertical offset between events to be poor. Relative errors for all relocated events were estimated using the singular value decomposition method and their average values are 4 m in latitude/longitude and 7 m in depth. The average shift

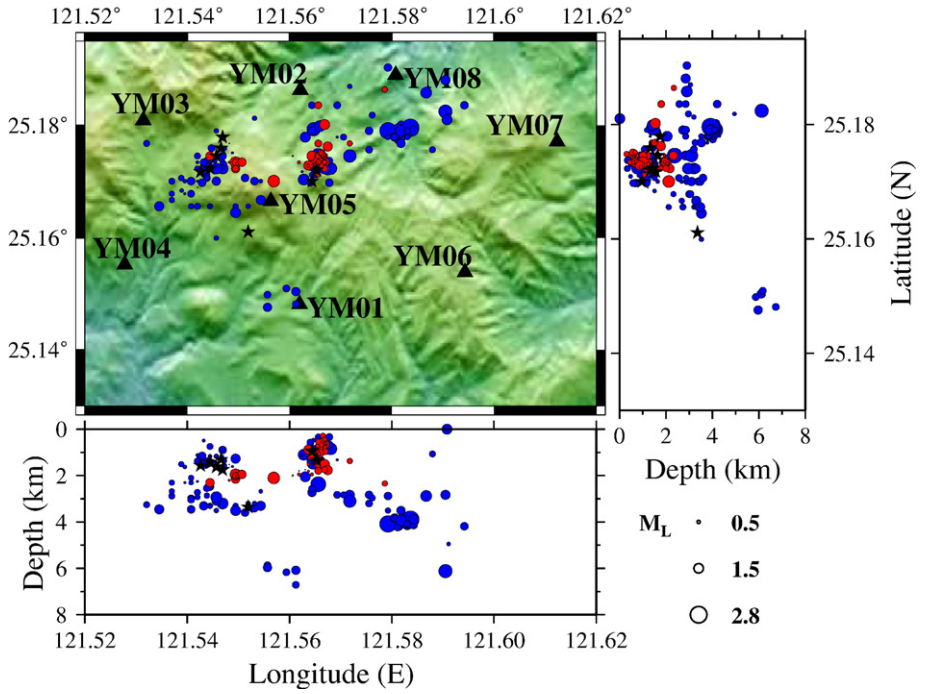


Fig. 11. Map of the TVG area showing the locations obtained using NONLINLOC and the minimum 1D model with station corrections. The blue circles indicate the isolated high frequency events, the red ones the spasmodic bursts events and the black stars the mixed frequency events. A scale relating the circle size to magnitude values is given at the lower right corner of the plot.

between locations obtained with NONLINLOC and those obtained from the relocation was ±11 m in latitude/longitude and ±18 m in focal depth, hence no significant change in the pattern of seismicity was observed. This result shows that NONLINLOC locations are already precise and well-constrained, a conclusion also reported by Lippitsch et al. (2005) in a similar seismicity study of Torfajökull volcano in Iceland.

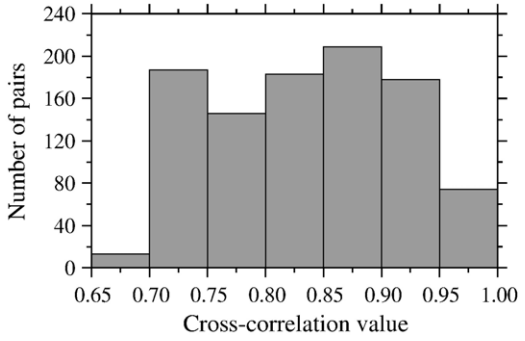


Fig. 12. Histogram showing the distribution of cross-correlation coefficients of P-phase waveforms used for determining differential traveltimes between events and common stations.

## 5. Discussion

### 5.1. Possible mechanisms of observed seismicity

High frequency events, similar to tectonic earthquakes, are caused by brittle failure of rock and constitute the main form of seismicity in the TVG area. Their occurrence is the result of the combined effect of the extensional regional stress field in northern Taiwan and the local stress field induced by the movement of hydrothermal fluids and/or magma. The relative contribution of these two stress fields can be determined by using two important parameters (Hill et al., 2003): (a) the ratio of the cumulative seismic moment to the geodetic moment derived from the observed deformation, (b) the frequency–magnitude distribution for an earthquake sample as represented by its *b*-value. The first parameter simply indicates which type of deformation (seismic versus aseismic) dominates, considering that mass transport is driven primarily by aseismic processes. The second parameter gives the relative proportion between small and large events in the sample under study. High *b*-values are thought to indicate high material heterogeneity and/or high thermal stress gradients in the vicinity of a magma chamber or conduit

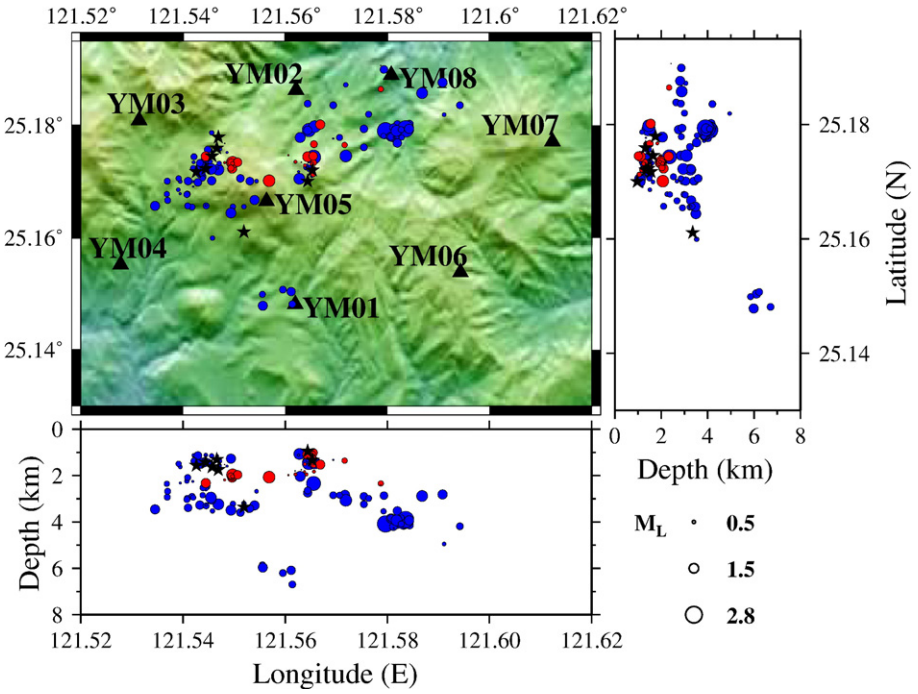


Fig. 13. Same as in Fig. 11 for the locations obtained using the double-difference method.

(Wyss et al., 1997; Wiemer and McNutt, 1997). For the TVG area, the first parameter cannot be estimated since there are no geodetic measurements for the period under study that could be used for the calculation of geodetic moment. However, the *b*-values reported for TVG in this and previous studies are much higher than those for the rest of Taiwan (Wang, 1988; Kim et al., 2005b) and imply the strong influence of hydrothermal fluid circulation on the local seismicity.

An observation that supports this conclusion is the frequent occurrence of another kind of high frequency seismicity, namely spasmodic bursts. These sequences of high frequency earthquakes are thought to be associated with a rupture cascade through a fracture mesh, driven by a transient increase in pore pressure (Hill, 1977; Hill et al., 1990; Hill and Prejean, 2005). Most of the hypocentres of spasmodic burst events in the TVG area are located at a depth interval of 0–2.5 km that coincides with large values of the $V_P/V_S$ ratio (~1.79), as indicated by the minimum 1D velocity model. Laboratory experiments have shown that this ratio is significantly higher in fluid-saturated rocks (Carcione and Cavallini, 2002), that supplies additional evidence for highly fractured, fluid-saturated rocks surrounding the focal area of spasmodic bursts.

Mixed frequency earthquakes represent only a small fraction of the observed seismicity, even though they can be considered as further evidence for the dominance of fluid-related processes in TVG. The commonest source model that has been used in order to explain the occurrence of mixed frequency events invokes two processes (Lahr et al., 1994; Gordeev and Senyukov, 2003; Ibáñez et al., 2003): first, the initial brittle failure of rock under high fluid pressure, that is responsible for the high frequency part of the observed signal; second, the flow of fluid into the void space resulting in the resonance of the newly formed crack and is responsible for the low frequency harmonic coda. Other proposed models include (a) the interference of two high frequency events that occur with a time delay dt, generating a harmonic waveform with regularly spaced spectral peaks every 1/dt Hz (Hough et al., 2000; Stroujkova and Malin, 2001); (b) brittle failure of rising melt under a sufficiently high strain rate (Goto, 1999; Tuffen et al., 2003).

The explanation given in (b) seems to be less likely for events occurring in TVG, since we have no evidence to suggest that a magma injection could have taken place during the period covered by this study. In order to try to distinguish which of the other two interpretations fits our observations better, we took a more detailed look of the characteristics of these signals in the time and frequency domains. For each mixed frequency event the Fourier spectrum of the vertical velocity component at

each station was calculated, using a standard FFT and a Hanning window that bracketed the main part of each waveform. Following that, the amplitude spectra were stacked so as to enhance the spectral peaks that were common and suppress those produced by path or site effects (Fig. 14). Two events (first two traces in Fig. 14) exhibited very regularly spaced peaks in their stacked spectra, every about 2 and 5 Hz respectively. However, no such pattern was apparent in the stacked spectra of the other events. An inspection of their waveforms recorded at the nearest stations, shows the existence of a large-amplitude secondary arrival that is delayed by 0.5 and 0.2 s for each event (Fig. 15). If one assumes that they represent the first arrival of a second seismic event, then it is expected that their spectrum will peak every 1/0.5=2 Hz and 1/0.2=5 Hz, as it is actually observed. Therefore, even though there is enough evidence to suggest that two of the mixed frequency events were caused by the interference of two high frequency earthquakes, the rest of them probably is better explained by the interaction of hydrothermal fluids with the bedrock.

### 5.2. A model for the volcano–hydrothermal system

A volcano–hydrothermal system can be defined as a system where heat and mass transfer from an igneous body (usually a magma chamber) to the Earth's surface, involving the convection and mixing of both magmatic and meteoric fluids (Hochstein and Browne, 2000). The magmatic fluids (gas exsolved from magma and/or water vapor) move from several kilometers depth through a network of cracks and ascend into the upper crust where they mix with infiltrated meteoric water and condense before they discharge on the surface. The manifestations of such a discharge can take the form of hot springs, hot lakes or fumaroles/solfataras. At the TVG area numerous hot springs and fumaroles with temperatures in the range of 90–200 °C attest to a vigorous hydrothermal activity. Most of these surface manifestations can be observed around the Tayiokeng area and at the NW part of the Chihsinshan edifice (Hsiaoyiokeng fumarole).

Based on the generic model described above, knowledge of local geology and the results of this

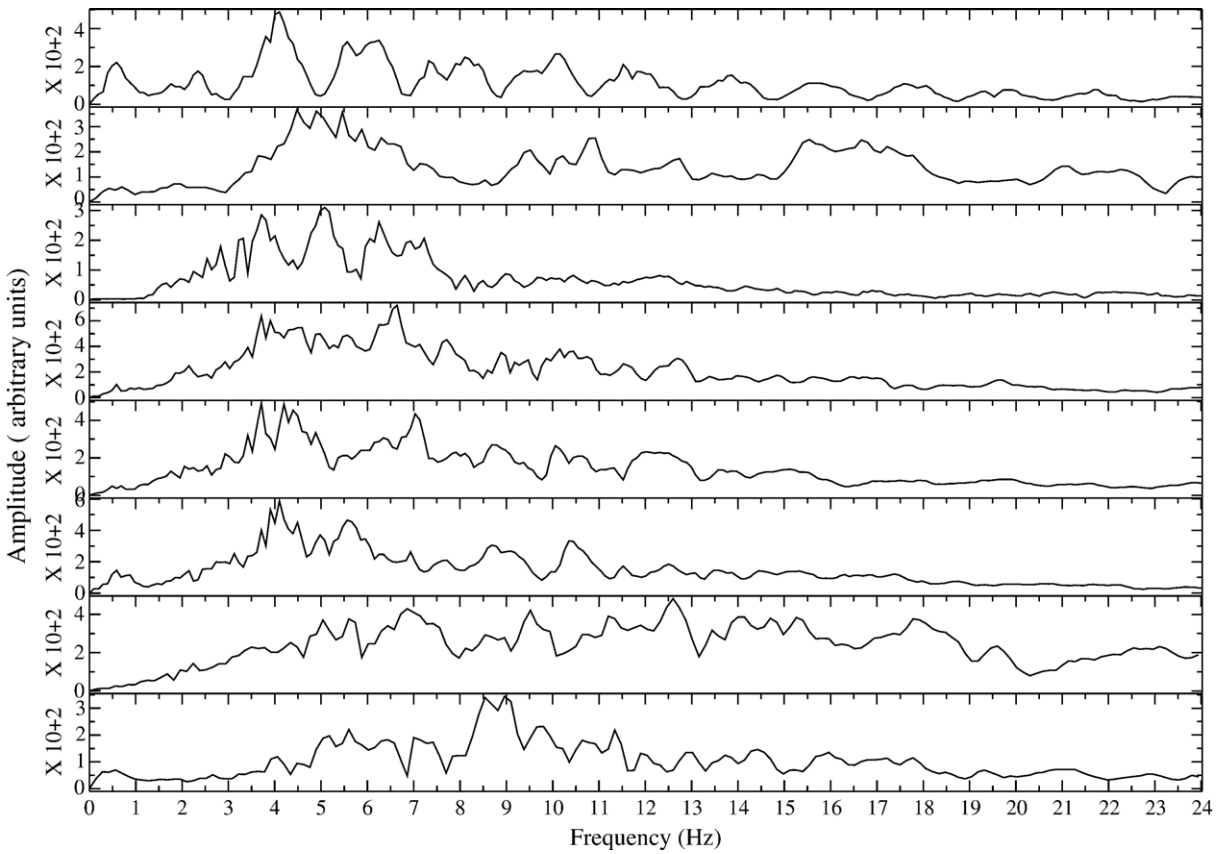


Fig. 14. Stacked amplitude spectra of the eight mixed frequency events that were recorded during the observation period. Note the spectral peaks every 2 and 5 Hz for the first and second trace respectively.

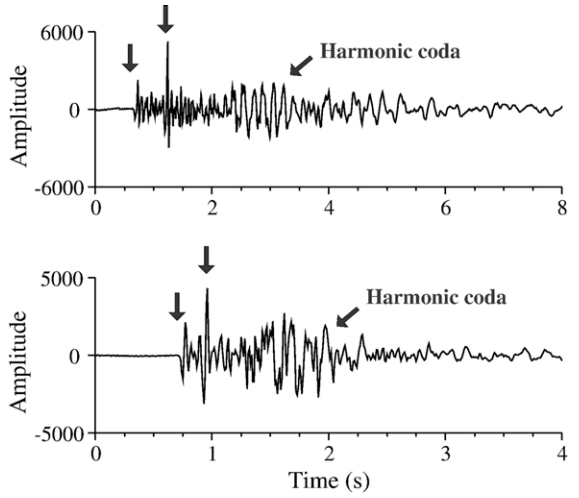


Fig. 15. Vertical velocity waveforms of two mixed frequency events recorded at station YM05 by a short-period sensor. The vertical arrows highlight the two large amplitude arrivals in the high frequency part of the signal.

study, we can construct a possible configuration of the volcano–hydrothermal system beneath the Chihsinshan–Tayiokeng area (Fig. 16). Surface geology indicates the existence of a system of extensional fractures around Chihsin-shan and near the Hsiaoyiokeng fumarole that probably function as a fluid feeding conduit (Chu et al., 1998). A zone of highly fractured and fluid-saturated rock may lie beneath Chihsinshan, extending to Tayiokeng, as evidenced by the occurrence of spasmodic bursts and elevated values of the $V_P/V_S$ ratio in the upper 3 km of the crust. This zone is fed with exsolved magmatic fluids through a system of conduits that connects it with a deeper magma source beneath TVG.

A crude estimate of the depth of the magma chamber can be obtained by considering the geothermal gradient of the area and the depth where the seismogenesis ceases. The maximum depth of seismogenesis at TVG does not exceed (with very few exceptions) 4 km, signifying a strong temperature or structural boundary at that depth. The former explanation may be more plausible than the latter one, if we take into account that the depth distribution of shallow earthquakes in Taiwan seems to be more correlated to the heat flow distribution rather than other factors (such as faulting mode, strain, geological composition and pore fluid pressure) (Wang et al., 1994). Assuming that the bottom of the seismogenic layer defines an isotherm, then for continental crust the temperature at 4 km should be in the range 350–400 °C (Ranalli and Rybach, 2005). This assumption is also supported by sub-surface temperature measurements taken from drilled holes at TVG that indicate a geothermal gradient of 100 °C $km^{-1}$ (Song et al., 2000b). Based on this information for the thermal structure, we can infer that the postulated magma chamber beneath TVG should be deeper than 7 km, since the temperature of rocks adjacent to a magma chamber seldom exceeds 700 °C (Gudmundsson, 1988).

### 5.3. A comparison with other Quaternary volcanoes

An interesting question that arises from this study is whether the characteristics observed at TVG can be considered as similar to those found in long-dormant

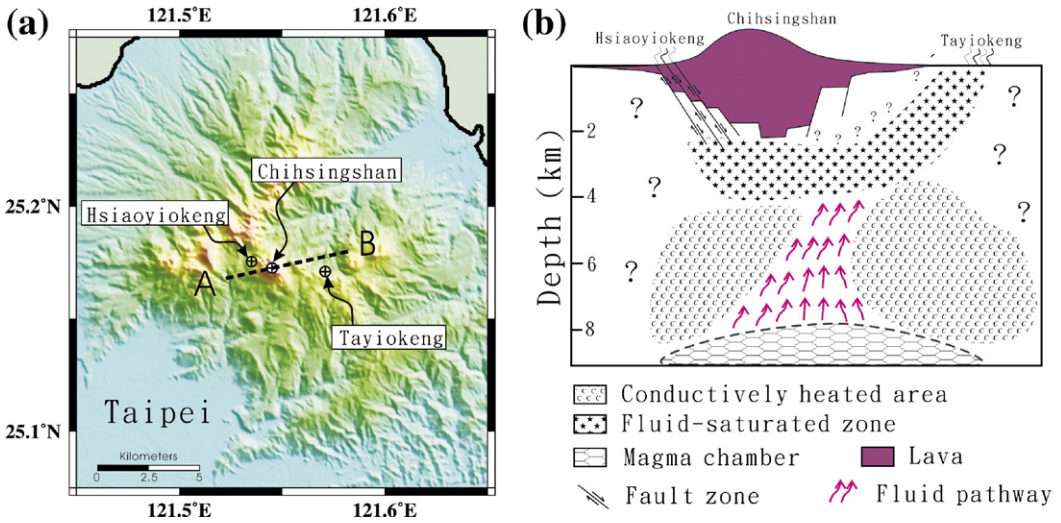


Fig. 16. Left panel: map of the TVG area showing the approximate orientation of the cross-section AB. Right panel: possible configuration of the volcano–hydrothermal system beneath the study area (see text for more details).

volcanoes that are expected to resume their eruptive activity in the future. Two such volcanoes that have been studied in some detail, are the Alban Hills volcano in central Italy (Amato et al., 1994; Chiarabba et al., 1997) and Mammoth Mountain in California (Hill et al., 1990; Hill and Prejean, 2005). Both of them exhibited a decreasing eruptive activity within the Quaternary period and their latest eruptions occurred 19 ka and 57 ka ago at Alban Hills and Mammoth Mountain respectively. In particular, chronostratigraphic studies at Alban Hills have shown that the volcano experienced a long dormancy period (~80 ka) interrupted by small scale eruptions (Marra et al., 2003). This pattern seems consistent with the observations cited earlier about the existence of similar eruptions at TVG during the last 20 ka.

Based on the results obtained after years of seismic and also geodetic monitoring of these two volcanic systems, their characteristics can be summarised as follows:

(1) Swarms of high frequency earthquakes form the majority of the observed seismicity and their duration can vary from several days to several years. Their local magnitudes are usually small (<3) but a few stronger events ($M_L \sim 4$) have taken place from time to time and were felt by the people living near these volcanoes. The maximum hypocentral depth for most of these high frequency events does not exceed 6–10 km for both volcanic areas, indicating a shallowing of the brittle–ductile transition presumably due to a high geothermal gradient.
(2) A small number of anomalous (low frequency) events has been observed at Alban Hills volcano after a seismic swarm that occurred during 1989–1990. The situation was similar at Mammoth Mountain with very few or no anomalous events before the onset of the 1989 seismic swarm and was followed by the progressive occurrence of spasmodic bursts, Deep (>10 km) Low Frequency (DLF) events and three very long period tremor episodes. One interpretation for this temporal pattern of anomalous events occurrence is that the swarms, through the brittle failure of rock, created the network of cracks necessary for the magmatic fluids to flow and to cause seismic disturbances like those observed.
(3) Frequent geodetic leveling surveys during the period 1927–1994 around Alban Hills volcano have revealed a maximum uplift of the order of 40 cm that was interpreted as evidence for the replenishment of its magma chamber from a deeper source. Similar measurements at Mammoth Mountain during the 1989 swarm have showed far smaller deformation (1–2 cm) and strain changes that can be modeled as a crack dislocation centered beneath Mammoth Mountain.

Our observations during 18 months of seismic monitoring of TVG can be viewed as qualitatively similar to what was observed at Alban Hills and Mammoth Mountain. However, there are a number of differences that have to be noted: (a) the maximum local magnitude at TVG was equal to 2.78 and therefore local residents living near this area never felt any of the ongoing seismic activity; (b) unlike TVG, Alban Hills and Mammoth Mountain each experienced a period of unrest that was followed by thousands of earthquakes occurring over a short time period; (c) even though four GPS stations have recently been deployed in the TVG area, there are no previous geodetic measurements that could reveal any aseismic deformation linked to the movement of hydrothermal fluids or even magma. As mentioned earlier, this latter point may be quite important since it was found that most of the deformation associated with the 1989 swarm at Mammoth Mountain developed aseismically (Langbein et al., 1993). Therefore, a longer observation period that would result in the accumulation of both seismic and deformation data is needed for a more accurate comparison with other Quaternary volcanoes in this respect.

### 5.4. A dormant or extinct volcano?

The traditional definition of an active volcano is the one with historical eruptions, or alternatively with historically documented eruptions (e.g. Smithsonian Institution, 1989). Szakáks (1994) argued that such a definition is inappropriate, on the grounds that the recorded history of volcanic eruptions represents a very different time span in different places around the world and that it ignores the diversity of volcano typology which in turn controls the eruption periodicities. The author proposes instead a phenomenological definition that states that a volcano can be considered active if its magmatic plumbing system is still working. In a similar way the IAEA guidelines for assessing volcanic hazards near nuclear facilities also takes into account the current status of the magmatic system of a volcano in order to classify it as capable/not capable for a future eruption (McBirney and Godoy, 2003).

This phenomenological definition relies on the detection of a number of symptoms that would imply the existence of a functional magma chamber beneath the volcano under study. Tilling (1989) recognised four such symptoms: (a) the occurrence of volcanoseismic signals, (b) high heat flow, (c) geochemical anomalies in the gas composition of the volcano–hydrothermal system, and (d)

deformation of the volcanic edifice. More recently, several authors have also suggested the occurrence of DLF events (Hasegawa and Yamamoto, 1994; Nakamichi et al., 2003; Power et al., 2004 among others) and the triggering of seismicity due to large distant earthquakes (Moran et al., 2004; Johnston et al., 2004; Husen et al., 2004 among others), as further diagnostics for detecting the reawakening of magmatic processes at a given volcano.

At TVG the first three symptoms mentioned above have been observed in the form of spasmodic bursts and low frequency signals, a high geothermal gradient and anomalous He isotope signatures of fumarole gas. During the period covered by this study our network did not record any DLF events. One possible reason for this may be the relatively short observation window, considering that such events are infrequent and their occurrence period may span several years (see for example Power et al., 2004). We also did not observe any seismicity increase after large distant events, including the December 26, 2004 (Mw ~ 9) Andaman–Sumatra earthquake. However, the results of the studies cited above have shown that several conditions have to be met (e.g. directivity of the large event, physicochemical properties of the magmatic system) for the occurrence of a triggering effect. In conclusion, even though there are some clear signs that TVG is not extinct as previously thought, the lack of more concrete evidence about the existence of magma beneath the area maintains the uncertainty regarding its status. Therefore, we prefer to use the term 'potentially active' for TVG, utilised by Szakáks (1994) to describe all such uneroded Quaternary volcanic systems.

In terms of volcanic hazards implications, it is likely that a future eruption at TVG may be a small one based on the evidence of previous small eruptions during the last 20 ka (Section 1.1). Such an eruption would be mostly composed of basaltic lava effusion and of a minor part of pyroclastic products. The hazards associated with such a scenario would be the direct threat posed to the visitors of the national park and to the nearby buildings due to possible forest fires or the lava flow itself. However, a danger more plausible than that of a future eruption is the occurrence of a prolonged seismic activity that would be accompanied by a number of locally felt events. This may inspire fear to the local society about a possible reawakening of the volcano and result in the mass movement of the population away from that area. Taking into account the proximity of TVG to the capital Taipei, such a development would have severe consequences for both the economic and social life, in a manner similar to the volcanoseismic crises at Long Valley caldera, California or Campi Flegrei in Italy. These cases have shown that a real-time seismic/deformation monitoring system would be able to give scientists enough hints so as to be able either to alert the authorities for an approaching eruption, or to reassure the population that there is no imminent danger.

## 6. Conclusions

The main conclusions of this study can be summarised as follows:

1. The seismicity in the TVG area consists mainly of high frequency earthquakes and a small number of mixed and low frequency events located near places of intense hydrothermal activity. A high *b*-value and an elevated $V_P/V_S$ ratio throughout the upper 3 km of the crust, demonstrate the influence of the hydrothermal fluid circulation on the local seismicity.
2. A crude estimate of the depth of the postulated magma chamber, derived from prior knowledge of the thermal structure of the area and the depth where seismogenesis ceases, points to a location deeper than 7 km.
3. A comparison of seismicity characteristics between TVG and two other well-studied dormant Quaternary volcanoes (Alban Hills in Italy; Mammoth Mountain in California) shows similar features. However, the lack of deformation data in TVG and the relatively short observation window covered by this study, do not allow a more accurate common pattern of behaviour to be identified.
4. Previous geochemical and geophysical studies, coupled with the results presented here, suggest that TVG may be a potentially active rather than an extinct volcano. This result may have severe implications for the safety of the nearby Taipei Metropolitan area and perhaps for the whole of northern Taiwan. Even in the best-case scenario where no eruption occurs, a prolonged seismic unrest near TVG may be enough to cause serious problems to both the economic and social life in the area.

## Acknowledgements

We would like to thank the National Research Council of Taiwan and the Yang-mingshan National Park for the financial support of the project and for a visiting scholar fellowship awarded to the first author. We are grateful to Frederik Tilmann and John VanDecar for allowing us to use their cross-correlation code. This manuscript benefited from constructive reviews by Philippe Lesage, Greg Waite and Haruhisa Nakamichi.

## References


Amato, A., Chiarabba, C., Cocco, M., di Bona, M., Selvaggi, G., 1994. The 1989–1990 seismic swarm in the Alban Hills volcanic area, central Italy. J. Volcanol. Geotherm. Res. 61, 225–237.

Carcione, J.M., Cavallini, F., 2002. Poisson's ratio at high pore pressure. Geophys. Prospect. 50, 97–106.

Chen, Y.L., 1995. Three-dimensional velocity structure and kinematic analysis in the Taiwan area, PhD thesis, National Central University, Jungli, Taiwan.

Chen, C.H., Lin, S.B., 2000. Distribution and significance of volcanic materials in sediments of the Taipei basin. J. Geol. Soc. China 43, 287–310.

Chen, C.H., Lin, S.B., 2002. Eruptions younger than 20 ka of the Tatun volcano group as viewed from the sediments of the Sungshan formation in the Taipei basin. West. Pac. Earth Sci. 2, 191–204.

Chen, K.J., Yeh, Y.H., 1991. Gravity and microearthquake studies in the Chinshan–Tamshui area, northern Taiwan. Terr. Atm. Ocean. Sci. 2, 35–50.

Chen, K.J., Yeh, Y.H., Yen, H.Y., Lin, C.H., 1995a. Seismological studies in the Chinshan fault area. Terr. Atm. Ocean. Sci. 4, 335–353.

Chen, C.H., Lee, C.Y., Lin, S.B., 1995b. The eruption age of volcanic ashes in the Wugu well, Taipei basin: constraints on mineral chemistry and $^{40}Ar/^{39}Ar$ dating. J. Geol. Soc. China 38, 371–381.

Chen, K.J., Lin, C.H., Hsieh, C.J., 2002. Mapping seismic attenuation structures of the volcanic area in northern Taiwan. West. Pac. Earth Sci. 2, 273–290.

Chiarabba, C., Amato, A., Delaney, P.T., 1997. Crustal structure, evolution and volcanic unrest of Alban Hills, central Italy. Bull. Volcanol. 59, 161–170.

Chu, C.J., Lee, C.T., Teng, L.S., 1998. Structural features and Quarternary tectonics of the Chinshan fault, northern Taiwan. J. Geol. Soc. China 41, 25–42.

Gordeev, E.I., Senyukov, S.L., 2003. Seismic activity at Koryakski volcano in 1994: hybrid seismic events and their implications for forecasting volcanic activity. J. Volcanol. Geotherm. Res. 128. doi:10.1016/S0377-0273(03)00256-7.

Goto, A., 1999. A new model for volcanic earthquake at Unzen volcano: melt rupture model. Geophys. Res. Lett. 26, 2541–2544.

Goldstein, P., Minner, L., 1996. SAC2000: seismic signal processing and analysis tools for the 21st century. Seismol. Res. Lett. 67, 39.

Gomberg, J.S., Shedlock, K.M., Roecker, S.W., 1990. The effect of S-wave arrival times on the accuracy of hypocentre estimation. Bull. Seismol. Soc. Am. 80, 1605–1628.

Gudmundsson, A., 1988. Effect of tensile stress concentration around magma chambers on intrusion and extrusion frequencies. J. Volcanol. Geotherm. Res. 35, 179–194.

Hasegawa, A., Yamamoto, A., 1994. Deep, low-frequency microearthquakes in or around seismic velocity zones beneath active volcanoes in northeastern Japan. Tectonophysics 233, 233–252.

Hill, D.P., 1977. A model for earthquakes swarms. J. Geophys. Res. 82, 1347–1352.

Hill, D.P., Prejean, S., 2005. Magmatic unrest beneath Mammoth Mountain, California. J. Volcanol. Geotherm. Res. 146. doi:10.1016/j.jvolgeores.2005.03.002.

Hill, D.P., Ellsworth, W.L., Johnston, J.S., Langbein, J.O., Oppenheimer, D.H., Pitt, A.M., Reasenberg, P.A., Sorey, M.L., McNutt, S.R., 1990. The 1989 earthquake swarm beneath Mammoth mountain, California: an initial look at the 4 May through 30 September activity. Bull. Seismol. Soc. Am. 80, 325–339.

Hill, D.P., Langbein, J.O., Prejean, S., 2003. Relations between seismicity and deformation during unrest in Long Valley Caldera, California, from 1995 through 1999. J. Volcanol. Geotherm. Res. 127. doi:10.1016/S0377-0273(03)00169-0.

Hochstein, M., Browne, P.R.L., 2000. Surface manifestations of geothermal systems with volcanic heat sources. Encyclopedia of Volcanoes, pp. 835–855.

Hough, S.E., Dollar, R.S., Johnson, P., 2000. The 1998 earthquake sequence south of Long valley caldera, California: hints of magmatic involvement. Bull. Seismol. Soc. Am. 90, 752–763.

Husen, S., Wiemer, S., Smith, R.B., 2004. Remotely triggered seismicity in the Yellowstone National Park region by the 2002 Mw 7.9 Denali Fault earthquake, Alaska. Bull. Seismol. Soc. Am. 94, S317–S331.

Ibáñez, J.M., Carmona, E., Almendros, J., Saccorotti, G., Del Pezzo, E., Abril, M., Ortiz, R., 2003. The 1998–1999 seismic crises at Deception island volcano, Antarctica. J. Volcanol. Geotherm. Res. 128. doi:10.1016/S0377-0273(03)00247-6.

Johnston, M.J.S., Prejean, S.G., Hill, D.P., 2004. Triggered deformation and seismic activity under Mammoth mountain in Long Valley Caldera by the 3 November 2002 Mw 7.9 Denali Fault earthquake. Bull. Seismol. Soc. Am. 94, S360–S369.

Kao, H., Jian, P.R., 2001. Seismogenic patterns in the Taiwan region: insights from source parameter inversion of BATS data. Tectonophysics 333, 179–198.

Kim, K.H., Chiu, J.M., Pujol, H., Chen, K.C., Huang, B.S., Yeh, Y.H., Peng, S., 2005a. Three dimensional $V_P$ and $V_S$ structural models associated with the active subduction and collision tectonics in the Taiwan region. Geophys. J. Int. 162. doi:10.1111/j.1365-246X.2005.02657.x.

Kim, K.H., Chang, C.H., Ma, K.F., Chiu, J.M., Chen, K.C., 2005b. Modern seismic observations in the Tatun volcano region of northern Taiwan: seismic/volcanic hazard adjacent to the Taipei metropolitan area. Terr. Atm. Ocean. Sci. 16, 579–594.

Kissling, E., 1995. Program VELEST User's Guide — Short Introduction, Institute of Geophysics, ETH Zurich.

Kissling, E., Ellsworth, W.L., Eberhart-Phillips, D., Kradolfer, U., 1994. Initial reference models in local earthquake tomography. J. Geophys. Res. 99, 19635–19646.

Kumagai, H., Chouet, B., 2000. Acoustic properties of a crack containing magmatic or hydrothermal fluids. J. Geophys. Res. 105, 25493–25512.

Lahr, J.C., Chouet, B.A., Stephens, C.D., Powers, J.A., Page, R.A., 1994. Earthquake classification, location, and error analysis in a volcanic environment: implications for the magmatic system of the 1989–1990 eruptions at Redoubt volcano, Alaska. J. Volcanol. Geotherm. Res. 62, 137–151.

Langbein, J.O., Hill, D.P., Parker, T.N., Wilkinson, S.K., 1993. An episode of reinflation of the Long Valley caldera, eastern California: 1989–1991. J. Geophys. Res. 98, 15851–15870.

Lin, C.H., Konstantinou, K.I., Liang, W.T., Pu, H.C., Lin, Y.M., You, S.H., Huang, Y.P., 2005a. Preliminary analysis of volcanoseismic signals recorded at the Tatun volcano group, northern Taiwan. Geophys. Res. Lett. 32, L10313. doi:10.1029/2005GL022861.

Lin, C.H., Konstantinou, K.I., Pu, H.C., Hsiu, C.C., Lin, Y.M., You, S.H., Huang, Y.P., 2005b. Preliminary results from seismic monitoring at the Tatun volcanic area of northern Taiwan. Terr. Atm. Ocean. Sci. 16, 563–577.

Lippitsch, R., White, R.S., Soosalu, H., 2005. Precise hypocentre relocation of microearthquakes in a high-temperature geothermal field: the Torfajökull central volcano, Iceland. Geophys. J. 160. doi:10.1111/j.1365-246X.2005.02467.x.

Lomax, A., Curtis, A., 2001. Fast, probabilistic earthquake location in 3D models using Oct-Tree importance sampling. Geophys. Res. Abstr. 3.

Lomax, A., Virieux, J., Volant, P., Berge-Thierry, C., 2000. Probabilistic earthquake location in 3D and layered models. In: Thurber, Rabinowitz (Ed.), Advances in Seismic Event Location, pp. 101–134.

Ma, K.F., Wang, J.H., Zhao, D., 1996. Three-dimensional seismic velocity structure of the crust and uppermost mantle beneath Taiwan. J. Phys. Earth 44, 85–105.

Marra, F., Freda, C., Scarlato, P., Taddeucci, J., Karner, D.B., Renne, P.R., Gaeta, M., Palladino, D.M., Triglia, R., Cavarretta, G., 2003. Post-caldera activity in the Alban Hills volcanic district (Italy): $^{40}Ar/^{39}Ar$ geochronology and insights into magma evolution. Bull. Volcanol. 65. doi:10.1007/s0044-002-0255-9.

Molina, I., Kumagai, H., Yepes, H., 2004. Resonances of a volcanic conduit triggered by repetitive injections of an ash-laden gas. Geophys. Res. Lett. 31. doi:10.1029/2003GL018934.

Moran, S.C., Power, J.A., Stihler, S.D., Sánchez, J.J., Caplan-Auerbach, J., 2004. Earthquake triggering at Alaskan volcanoes following the 3 November 2002 Denali Fault earthquake. Bull. Seismol. Soc. Am. 94, S300–S309.

McBirney, A., Godoy, A., 2003. Notes on the IAEA guidelines for assessing volcanic hazards at nuclear facilities. J. Volcanol. Geotherm. Res 126. doi:10.1016/S0377-0273(03)00113-6.

McNutt, S.R., 1996. Seismic monitoring and eruption forecasting of volcanoes: a review of the state-of-the-art and case histories. In: Scarpa, Tilling (Ed.), Monitoring and Mitigation of Volcanic Hazards, pp. 100–146.

Nakamichi, H., Hamaguchi, H., Tanaka, S., Ueki, S., Nishimura, T., Hasegawa, A., 2003. Source mechanism of deep and intermediate-depth low-frequency earthquakes beneath Iwate volcano, north-eastern Japan. Geophys. J. Int. 154, 811–828.

Power, J.A., Stihler, S.D., White, R.A., Moran, S.C., 2004. Observations of deep long-period (DLP) seismic events beneath Aleutian arc volcanoes; 1989–2002. J. Volcanol. Geotherm. Res. 138. doi:10.1016/j.jvolgeores.2004.07.005.

Ranalli, G., Rybach, L., 2005. Heat flow, heat transfer and lithosphere rheology in geothermal areas: features and examples. J. Volcanol. Geotherm. Res. 148. doi:10.1016/j.volgeores.2005.04.010.

Rau, R.J., Wu, F.T., 1995. Tomographic imaging of lithospheric structures under Taiwan. Earth Planet. Sci. Lett. 133, 517–532.

Roecker, S.W., Yeh, Y.H., Tsai, Y.B., 1987. Three-dimensional P and S wave velocity structures beneath Taiwan: deep structure beneath an arc-continent collision. J. Geophys. Res. 92, 10547–10570.

Shin, T.C., 1993. The calculation of local magnitude from the simulated Wood–Anderson seismograms of the short-period seismograms in the Taiwan area. Terr. Atm. Ocean. Sci. 4, 155–170.

Smithsonian Institution, 1989. Global Volcanism 1975–1985. Prentice Hall, New Jersey.

Song, S.R., Lo, H.J., 1995. The source and origin of the volcanoclastics in Linkou formation of northern Taiwan. J. Geol. Soc. China 38, 287–314.

Song, S.R., Tsao, S., Lo, H.J., 2000a. Characteristics of the Tatun volcanic eruptions, north Taiwan: implications for a cauldron formation and volcanic evolution. J. Geol. Soc. China 43, 361–378.

Song, S.R., Yang, T.F., Yeh, Y.H., Tsao, S.J., Lo, H.J., 2000b. The Tatun volcano group is active or extinct? J. Geol. Soc. China 43, 521–534.

Stroujkova, A., Malin, P., 2001. Multiple ruptures for Long valley microearthquakes: a link to volcanic tremor? J. Volcanol. Geotherm. Res. 106, 123–143.

Szakáks, A., 1994. Redefining active volcanoes: a discussion. Bull. Volcanol. 56, 321–325.

Tarantola, A., Valette, B., 1982. Inverse problems = quest for information. J. Geophys. 50, 159–170.

Teng, L.S., 1996. Extensional collapse of the northern Taiwan mountain belt. Geology 24, 949–952.

Tilling, R.I., 1989. Volcanic hazards and their mitigation: progress and problems. Rev. Geophys. 27, 237–269.

Tsao, S.J., Song, S.R., Lee, C.Y., 2001. Geological implications of Lahar deposits in the Taipei basin. West. Pac. Earth Sci. 1, 199–212.

Tuffen, H., Dingwell, D.B., Pinkerton, H., 2003. Repeated fracture and healing of silicic magma generate flow banding and earthquakes? Bull. Geol. Soc. Am. 31, 1089–1092.

VanDecar, J.C., Crosson, R.S., 1990. Determination of teleseismic relative phase arrival times using multi-channel cross-correlation and least squares. Bull. Seismol. Soc. Am. 80, 150–169.

Waldhauser, F., Ellsworth, W.L., 2000. A double-difference earthquake location algorithm: method and application to the northern Hayward fault, California. Bull. Seismol. Soc. Am. 90, 1353–1368.

Waldhauser, F., 2001. HypoDD: a Program to Compute Double-Difference Hypocentre Locations. U.S. Geological Survey, Open File Report, vol. 01-113.

Wang, J.H., 1988. *b*-values of shallow earthquakes in Taiwan. Bull. Seismol. Soc. Am. 78, 1243–1254.

Wang, J.H., Chen, K.C., Lee, T.Q., 1994. Depth distribution of shallow earthquakes in Taiwan. J. Geol. Soc. China 37, 125–142.

Wang, K.L., Chung, S.L., Chen, C.H., Shinjo, R., Yang, T.F., Chen, C.H., 1999. Post-collisional magmatism around northern Taiwan and its relation with opening of the Okinawa trough. Tectonophysics 308, 363–376.

Wiemer, S., McNutt, S.R., 1997. Variations in the frequency–magnitude distribution with depth in two volcanic areas: Mt. St Helens, Washington and Mt. Spurr, Alaska. Geophys. Res. Lett. 24, 189–192.

Wyss, M., Shimazaki, K., Wiemer, S., 1997. Mapping active magma chambers by b values beneath the off-Ito volcano, Japan. J. Geophys. Res. 102, 20413–20422.

Wu, F.T., Rau, R.J., Salzberg, D., 1997. Taiwan orogeny: thin-skinned or lithospheric collision? Tectonophysics 274, 191–220.

Yang, C.H., Shei, T.C., Lue, C.C., 1994. Gravity and magnetic studies in the Tatun volcanic region. Terr. Atm. Ocean. Sci. 5, 499–514.

Yang, T.F., Sano, Y., Song, R.S., 1999. $^{3}He/^{4}He$ ratios of fumaroles and bubbling gases of hot springs in Tatun volcano group, north Taiwan. Nuovo Cim. 22, 281–285.

Yeh, Y.H., Liu, C.C., Lin, C.H., Liu, C.C., Yen, H.Y., 1998. Geophysical monitoring of volcano activities at Mt. Tatun. Eos Trans. AGU 79 (24), W124 (Westrn Pac. Geophys. Meet. Suppl.).

Yu, S.B., Chen, H.Y., Kuo, L.C., Lallemand, S.E., Tsien, H.H., 1997. Velocity field of GPS stations in the Taiwan area. Tectonophysics 274, 41–59.